AIMS Materials Science, 12(2): 203–223.
DOI: 10.3934/matersci.2025011
Received: 28 November 2024
Revised: 22 January 2025
Accepted: 07 February 2025
Published: 13 March 2025

http://www.aimspress.com/journal/Materials

Research article

The effect of solid-state process and heat treatment on the fatigue life of RHA-reinforced AA6061 chip-based recycled composite

Amin Shah Omar, Shazarel Shamsudin*, Yahya M. Altharan, Mohd Amri Lajis, and Nur Kamilah Yusuf

Sustainable Manufacturing and Recycling Technology, Advanced Manufacturing and Materials Center (SMART-AMMC), Universiti Tun Hussein Onn Malaysia, Parit Raja 86400, Malaysia

* **Correspondence:** Email: shazarel@uthm.edu.my.

Abstract: The direct recycling method has gained increasing attention due to its potential to reduce waste and costs while being environmentally friendly. This study investigated the effect of hot extrusion and heat treatment on AA6061 aluminium chips recycled and reinforced with 5 wt.% rice husk ash (RHA) burned at 1100 °C. The cold compacted billets were preheated at 550 °C for 2 h before being extruded at 300 °C. Half of the extruded billets were heat treated for 2 h at 530 °C, rapidly quenched in water at 26 °C, and then underwent artificial aging at 175 °C for 4 h. The samples were tested for relative density, ultimate tensile strength (UTS), hardness, and fatigue life, and examined for microstructure. Comparisons were made between heat-treated, untreated, and the as-received samples. The highest strength of 145.65 MPa, hardness of 64.78 HV, and density of 2.64 g/cm^3 were observed in the treated samples. Heat-treated samples recorded higher fatigue limits than non-treated ones. Basquin's equation was used to predict the fatigue life of the composite at an untested stress amplitude. Energy dispersive spectroscopy (EDS) analysis revealed that treated samples constitute 83.29% of the total composition, followed by magnesium at 7.32%, and oxygen at 6%. Atomic force microscopy (AFM) analysis showed that the grain length of the heat-treated sample ranged from 0.792 to 0.894 µm, which is larger than the grain size of the untreated samples. In conclusion, hot extrusion and heat treatment effectively improve the microstructure and mechanical properties of the chip-based RHA-reinforced composite.

Keywords: AA6061 chips; extrusion; microstructure; heat treatment; RHA; UTS

1. Introduction

The modern world constantly seeks ways to turn waste into valuable resources as efficiently as possible. Solid-state recycling is a process that allows for the recycling of aluminium waste without the remelting process [1]. This method, also known as a direct conversion, has recently gained popularity due to its potential to reduce energy consumption, emissions, and environmental impact compared to conventional aluminium recycling methods [2]. In conventional methods, aluminium scrap is melted and reformed, which requires high energy inputs and emissions [3]. In contrast, solid-state aluminium recycling directly converts aluminium scrap and chips into a semi-finished and finished product without melting. Solid-state recycling enables the reuse of materials that would otherwise be discarded, thereby conserving raw materials [4]. Conversion recycling has the potential to diminish greenhouse gas emissions by lowering the energy and material demands associated with traditional production methods [4].

Moreover, the literature indicates that conversion recycling can produce products with mechanical and physical properties comparable to those produced through conventional methods [5–9]. Consequently, solid-state aluminium recycling methods, such as hot forging, hot extrusion, equal channel angular pressing (ECAP), and powder metallurgy, can offer a more sustainable and cost-effective solution for aluminium recycling in the industrial sector [10,11]. The hot extrusion method utilized in this research is commonly applied in aluminium chip recycling, as it omits the heating phase process [12,13]. Based on the deformation route and process parameters, the mechanical properties of aluminium chip-based extrudates are comparable to or superior to those of casted billets [14]. Through the hot extrusion process, the extruded profile is shaped by forcing it through a die under high pressure [15]. Hot extrusion facilitates enhanced control over the shape and properties of the semi-finished product, rendering it an effective method for producing chip-based products [12].

The development of aluminium metal matrix composite (AMC) is a major milestone in material history. AMCs were developed to enhance the properties of aluminium alloy and meet the demands of modern engineering products. The process of alloying aluminium with other materials can improve its mechanical properties, such as increasing strength, hardness, and resistance to corrosion [16]. Rice husk, a byproduct of rice production, is used as a reinforcement in AMCs to improve mechanical properties such as strength, stiffness, and wear resistance [17]. Rice husk ash (RHA) is a waste material that generates methane and carbon dioxide. Utilizing it as a reinforcing fiber in the recycling process can mitigate the environmental impact of this waste [18]. Researchers reported that incorporating RHA can significantly enhance the mechanical and physical properties of recycled aluminium parts [19–22]. The combustion temperature significantly influences the properties of RHA utilized as a reinforcement in recycled AA6061 chips. Increased burning temperatures typically lead to elevated silica content, reduced particle size, and diminished impurities, thereby improving the mechanical and physical properties of the resultant composite material [22,23]. Rice husk may not achieve complete carbonization at low combustion temperatures, producing oxygen-containing functional groups on its surface. These functional groups can interfere with rice husk and aluminium matrix bonding, reducing composite

material performance [24]. This work involved the reinforcement of AA6061 chips with RHA, which are subsequently processed by a hot extrusion method.

Recycled composites often have limited mechanical and physical properties. The fatigue life of reinforced composites is critical as fatigue failure can frequently happen abruptly and result in severe outcomes [25]. The process occurs by initiating and propagating cracks perpendicular to the direction of maximum cyclic stress [26]. Therefore, this study investigates the fatigue behavior of the recycled composite material. Heat treatment was conducted to examine the composite's hardness, density, tensile properties, microstructure, and fatigue behavior and to compare the results with non-heat-treated samples.

This research aims to recycle AA6061 aluminium chips reinforced with RHA utilizing a hot extrusion process followed by solution heat treatment and artificial aging. The objective is to investigate the impact of heat treatment on the properties of the extruded composite. A predictive fatigue life model was also established for the chip-based recycled composite based on optimal process parameters. The developed AMC provides new engineering applications for the construction sector in Malaysia. The findings of this study can highlight the potential of direct recycling technologies to conserve energy and natural resources while also encouraging further research in this field.

2. Methods and methods

2.1. Materials preparation

The chips were prepared from an AA6061 aluminium block by a Sodick-MC430L high-speed milling machine with a 4 mm average length. The machined chips were cleaned to remove contaminants such as oil, grease, or dirt in acetone (C_3H_6O) solution with an ultrasonic S 60H bath and dried thoroughly at 60 °C for 2 h following ASTM G131-96 to prevent corrosion during storage. The rice husk was washed with water to remove dirt and dust, dried for 1 h at 200 °C, and then burned at 1100 °C for 60 min. The collected rice husk ash was ground for 30 min at 350 rpm using a Fritsch planetary mono mill machine. The collected RHA and chips were blended for one hour at 25 rpm speed by a 3D mixer.

Table 1. The selected milling parameters.

No.	Parameter	Value
1	Feed rate	0.05 mm/tooth
2	Cutting speed	1100 m/min
3	Cutting depth	1.0 mm

2.2. Rule of mixing

RHA is mixed with chips to develop a homogeneous composite, ensuring uniform distribution. The mixing process was conducted based on the weight fraction of the particulate and matrix utilizing the rule of mixing composite and theoretical density, as expressed in Eqs 1–3.

$$\rho = \frac{W}{v} \tag{1}$$

$$W_c = W_a + W_m \tag{2}$$

$$\rho_c = \rho_a V_a + \rho_a V_m \tag{3}$$

where w and ρ_c are the weight and composite density, V refers to volume, and subscripts a and m represent RHA and the metal matrix, respectively.

2.3. Hot extrusion process

Hot extrusion is a severe plastic deformation (SPD) process where compacted billet is pressed through a flat face die by ram using hydraulic force. The chip/RHA mixture was weighed according to the mixing rule and cold compacted four times at a pressure of 35 tons to form billets. Before extrusion, each billet was heated in the hot extrusion machine's furnace at 550 °C for 2 h for annealing. The machine container was heated up to 300 °C during extrusion to reduce billet heat loss during container contact. The extruded metal flowed through the die opening in a round billet shape. The hot extrusion process parameter settings used are listed in Table 2.

Table 2. Extrusion process parameter settings.

Extrusion parameters	Value
Die shape	Round
Extrusion speed (mm/s)	4
Billet diameter (mm)	30
Die orifice diameter (mm)	13
Extrusion ratio, R	5.4
Die/container assembly temperature (°C)	300
Billet preheating temperature (°C)	550
Billet preheating duration (h/s)	2

2.4. Heat treatment process

Ten billets were prepared based on the optimal parameters determined from the preliminary results, which included 5% RHA content burned at 1100 °C, an extrusion temperature of 550 °C, and a preheating duration of 2 h. Additionally, one billet was extruded without RHA addition (base alloy) as a reference sample. Precipitation hardening was applied to five extrudates to investigate the composite's hardness, density, tensile strength, fatigue behavior, and microstructure. The results were then compared to those of the non-heat-treated billets. The five extrudate samples were subjected to solution heat treatment and artificial aging for 2 and 4 h at 530 and 175°C, respectively, as depicted in Figure 1. Subsequently, the samples were rapidly quenched in water at the rate of 100 °C/s. These two categories of samples were denoted by heat-treated (HT) and non-heat-treated samples (NHT). The heat-treated and untreated samples are shown in Figure 2.

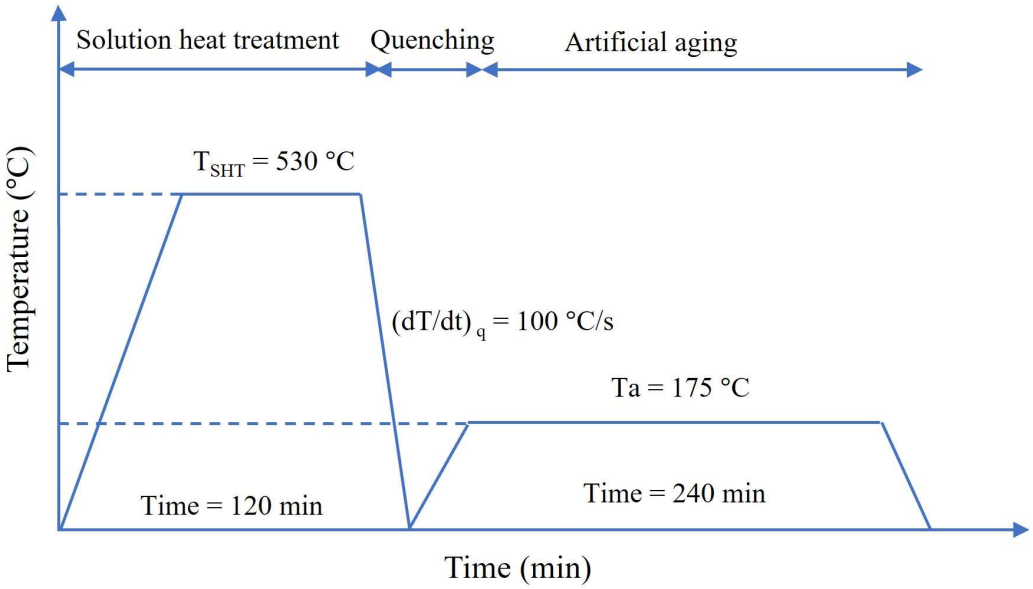

Figure 1. The temperature diagram of heat treatment.

Figure 2. Extrudate samples (a) before heat treatment and (b) after heat treatment.

2.5. Experimental tests

The tensile specimens were machined per the ASTM-E8M-04 standard, as elucidated in Figure 3. The tensile and yield strength (YS) of the RHA-chip composite were determined before the fatigue life test was conducted. Samples were tensile-tested by a universal testing machine (Shimadzu EHF-EM0100K1-020-0A). The ultimate tensile strength (UTS) values of 0.50%, 0.60%, 0.70%, 0.80%, and 0.90% were used for fatigue testing. The fatigue test was performed using an Instron 8801 Fatigue Machine at 20 Hz frequency with a maximum of 10^7 cycles as per ASTM E466 in Figure 4. The hardness measurement was carried out by a Vickers microhardness tester, with a predetermined load of 2.943 N for 10 s as per ASTM E384-11 standard by means of a pyramid-shaped diamond. The Vickers hardness test is useful for testing microstructure surface materials as the indenter is much smaller than the indenters used in other hardness testing methods. The microstructure and energy dispersive spectroscopy (EDS) were carried out by scanning electron microscope (JSM-T330A SEM) and AFM.

The fatigue fracture features were examined using a Hitachi SU1510 optical microscope (Olympus BX60M) following standard ASTM E3 and ASTM E340. The test specimens were ground with 240, 600, and 1200 SiC paper for 3 min. All specimens were treated with TEXPAN polishing 1 and 2 μm NAPPAD for 540 s and etched for 2 min at 12 V DC using Barker's reagent. This procedure assists in revealing the microstructure of a specimen and analyzing its topography. The density of hybrid composite specimens from HT and NHT was calculated and measured based on Archimedes' principle. Density measurements were conducted in distilled water for all the specimens using the HR-250AZ Compact Analytical Balance Density Determination Kit. The balance was set to zero prior to weighing the samples. Small billet pieces were weighed in distilled water and air to determine their weight in different environments. The density was then calculated using Eq 4 based on the measured room temperature.

$$\rho = \frac{m}{|V|} \times density\ of\ distilled\ water\ at\ a\ certain\ temperature \tag{4}$$

where ρ, m, and V are density, mass in air, and volume in liquid, respectively.

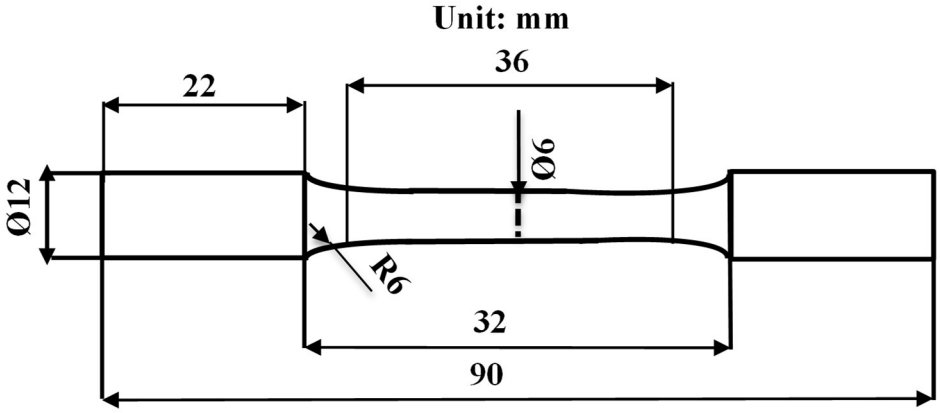

Figure 3. Tension test specimen dimension in mm (ASTM E8M-04).

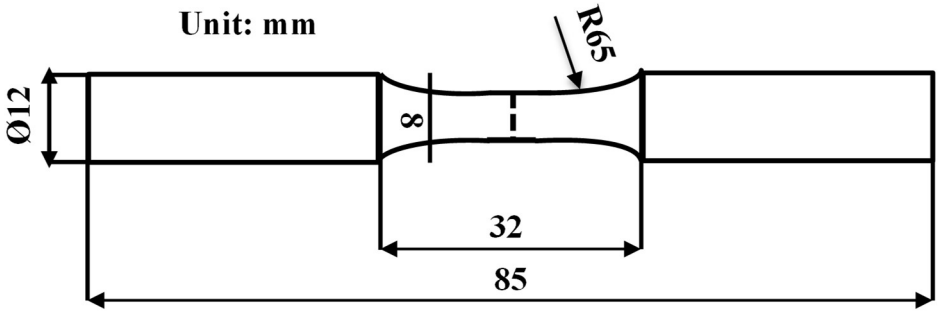

Figure 4. Fatigue test specimen dimension in mm (ASTM E466-15) (standard test methods for tension testing of metallic materials).

3. Results and discussion

3.1. Ultimate tensile strength

The UTS result of three treated samples and one untreated sample is shown in Table 3. The NHT sample showed lower UTS results compared to heat-treated samples. A 45.7% increase in UTS was observed between the NHT and HT samples. Heat treatment had a significant impact on the composite's strength. These findings demonstrated a substantial change in the properties of the heat-treated samples. Hot extrusion and heat treatment significantly affect the composite microstructure and mechanical properties. Hot extrusion densifies aluminium chips to strengthen the welding and reinforcement particle bonding, facilitating porosity reduction to enhance composite strength and ductility. Heat treatment further refines the microstructure by promoting grain growth and reducing residual stresses, thereby improving strength, ductility, and fatigue performance. Heat-treated samples exhibited improved UTS relative to untreated samples, rendering them appropriate for construction applications and automotive components.

Table 3. Results of UTS, YS, and Young's modulus.

Sample	UTS (MPa)	YS (MPa)	Young's modulus (GPa)
S1-HT	139.77	112.32	43.9
S2-HT	134.38	117.17	42.2
S3-HT	140.83	93.0	87.0
S4-NHT	96.65	79.8	87.7

3.2. Microhardness

The microhardness result of HT, NHT, and the reference samples is shown in Figure 5. The ten hot extruded samples produced based on optimum parameters (5% RHA, 1100 °C RHA, 550 °C Tp, and 2 h preheating time) were divided into two groups of five samples each. In addition, one billet was extruded without RHA addition (base alloy) as a reference sample. The samples of the two categories were denoted by HT and non-heat-treated samples (NHT). Figure 5 illustrates the significant positive impact of heat treatment on the hardness of the extruded samples. The HT samples demonstrated a higher hardness value than the NHT samples. The highest hardness of the NHT samples was 51.36 HV, whereas the maximum of the HT samples was 64.78, with a significant increase of 26%. The maximum hardness of the heat-treated reference sample without RHA addition was 60 HV.

On the other hand, the maximum hardness of the HT sample reinforced with 5% RHA was 64.78 HV, representing a slight increase of 8%. The improvement in the hardness of the hybrid composite can be attributed to the even distribution of RHA particles throughout the matrix material. Despite being produced under the same extrusion conditions, heat treatment and rapid quenching resulted in better hardness in the HT samples than in the NHT samples. The aging process facilitates the precipitation of fine, uniformly dispersed reinforcing phases like Mg_2Si, which enhance mechanical properties. These precipitates enhance the matrix by hindering dislocation movement improving tensile strength and hardness. Adding RHA particles further refine the matrix structure, facilitating a more homogenous

distribution of Mg_2Si precipitates. This combined effect substantially boosts both tensile strength and hardness.

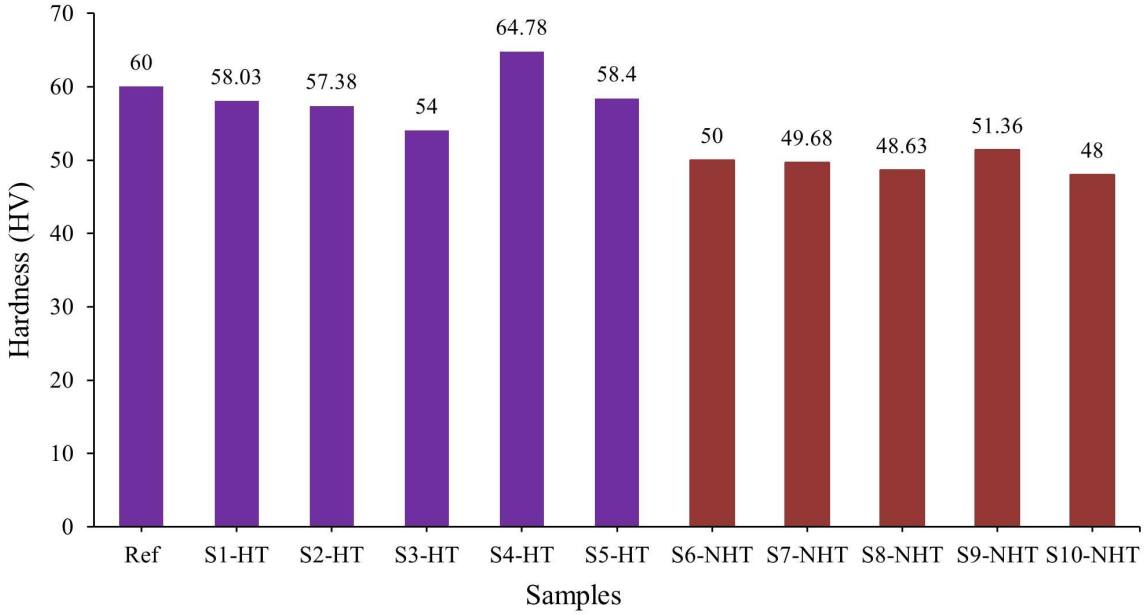

Figure 5. The hardness results of heat-treated and non-treated samples.

3.3. Density measurement analysis

As seen in Figure 6, the NHT samples recorded a lower density than the HT samples. The heat treatment slightly improved the density of the samples. The density measurement of the reference sample is 2.7 g/cm^3, while the highest density of the HT sample S5-HT is almost 2.64 g/cm^3. However, both samples were extruded under similar conditions. This is due to the higher density of the AA6061 chip compared to RHA. In short, the average density measurement of the heat-treated specimens was 2.62 g/cm^3, 3% lower than the as-received sample density. In contrast, untreated samples have an average density value of 2.56 g/cm^3.

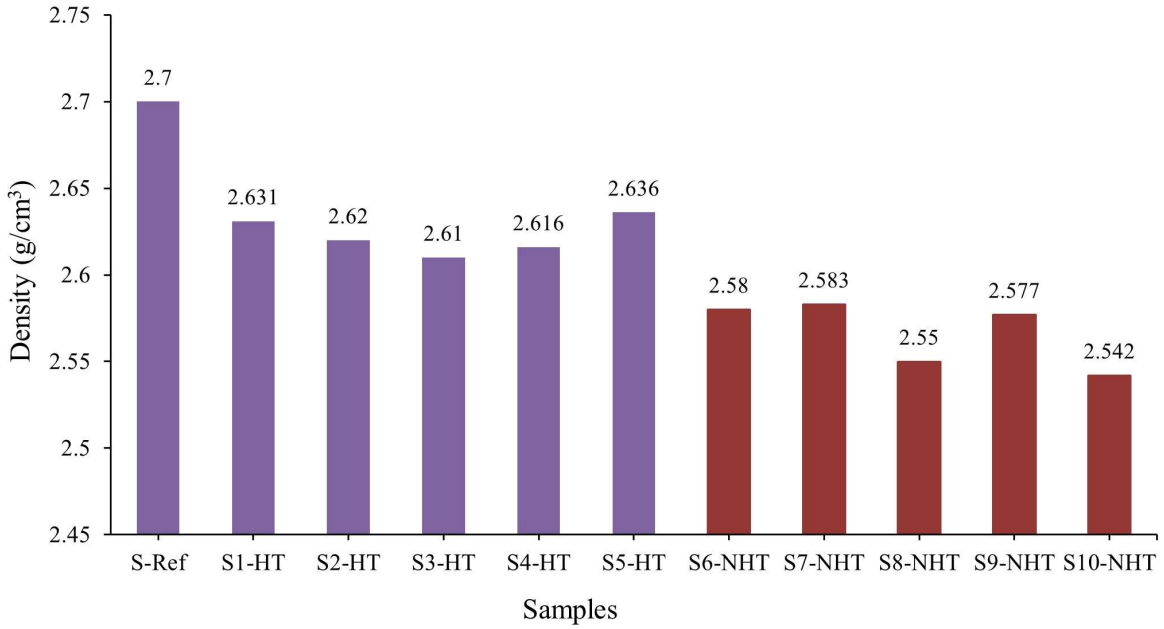

Figure 6. Density measurement of HT and NHT samples.

3.4. Fatigue behavior analysis

The high cycle fatigue (HCF) testing was carried out per ASTM E466-15 standard with a maximum of 10^7 cycles. As can be seen in Table 4, the sample S1-HT endured 8.74×10^5 cycles before failure at a stress level of 90 MPa. S6-NHT failed at 1,632,538 cycles when 72 MPa stress was applied. Meanwhile, the HT sample that was subjected to the same stress level withstood 2,208,121 cycles. S3-HT demonstrated a significant increase in endurance, reaching 3.189×10^6 cycles when tested at a stress level of 65 MPa. However, the S7-NHT sample failed at 2.6178×10^6 cycles. At 58% yield strength and 62 MPa stress magnitude, S4-HT endured a load of 5.5216×10^6 cycles before failure. When applied stress was reduced to 60 MPa, the heat-treated sample did not experience fatigue failure even at 10^7 cycles. However, when applied stress was reduced to 58 MPa, the untreated sample experienced fatigue failure at 8.97×10^6 cycles. The untreated samples recorded lower fatigue limits than heat-treated ones, as depicted in Figure 7. Poor chip bonding and microcracks in the untreated extrudate caused the early failure.

Table 4. Fatigue behavior test of HT and NHT samples.

Heat-treated samples			Non-heat-treated sample		
Sample	Stress 1 (σ_1)	Cycle (N_1)	Sample	Stress 2 (σ_2)	Cycle (N_2)
S1-HT	90.1	873,998	S6-NHT	72	1,632,538
S2-HT	75	2,208,121	S7-NHT	65	2,617,872
S3-HT	65	3,189,085	S8-NHT	62	4,433,242
S4-HT	62	5,521,562	S9-NHT	58	6,206,731
S5-HT	60	10,000,000	S10-NHT	56	8,971,416

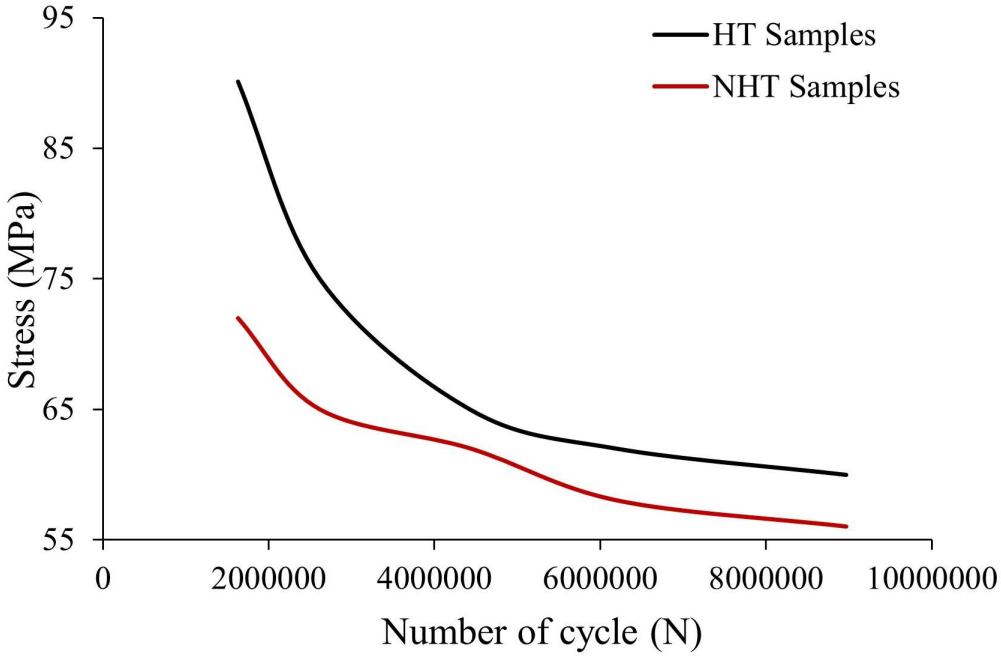

Figure 7. S-N curve of heat-treated and non-treated samples.

3.5. Modeling of fatigue life using Basquin's equation

Basquin's equation is a mathematical model that describes the relationship between the stress amplitude (σ) and the number of cycles to failure (Nf) for material under fatigue loading. This relationship is represented by Eq 5. The Basquin equation is commonly used as an established empirical model for predicting fatigue life in high-cycle fatigue, especially for metallic materials and composites [27,28] The Basquin equation effectively models high-cycle fatigue behavior due to its simplicity and strong correlation between stress amplitude and fatigue life [29]. Its simplicity and the ability to establish a log-log linear relationship between stress amplitude and fatigue life make it a practical and reliable tool [30]. The high R^2 values (92.1%–99.84%) from regression analyses validate its applicability, enabling accurate predictions of the composite's fatigue life at unphysically tested stress amplitudes, which is essential for practical applications.

The Basquin equation takes the form:

$$\sigma = A(Nf)^b \tag{5}$$

where A is the fatigue strength coefficient, and b represents the fatigue strength exponent, which describes the slope of the curve on a log-log plot of S-N. A fitted line plotting program was utilized to determine the Basquin equation constants (A and b). This process involved identifying the values of data points on the S-N curve, as presented in Table 5, which summarizes the results of the high-cycle fatigue test.

Minitab 21 statistical software was used to generate a curvilinear fitted line plot between the data points to determine the values of A and b that best fit the data using a regression equation. Basquin's equation was used to predict the number of cycles to failure for any given stress amplitude based on b

and *A* values. Thus, the fatigue life of the chip-RHA composite can be predicted at a stress amplitude that was not physically tested. In a log-log plot, the *x*-axis represents log10 of stress amplitude (response), and the *y*-axis represents log10 of the number of cycles (predictor). The relationship described is inversely proportional: as the log of stress amplitude increases, the log of cycles decreases, and vice versa.

Table 5. Log stress amplitude and the number of cycles.

Heat-treated samples			Untreated samples		
Sample	Log stress 1 (σ_1)	Log cycles (N_1)	Sample	Log stress 2 (σ_2)	Log cycle (N_2)
S1-HT	1.955	5.942	S6-NHT	1.857	6.213
S2-HT	1.875	6.344	S7-NHT	1.813	6.418
S3-HT	1.813	6.504	S8-NHT	1.792	6.647
S4-HT	1.792	6.742	S9-NHT	1.763	6.793
S5-HT	1.778	7.000	S10-NHT	1.748	6.923

Figures 8 and 9 present the fitted line plots of stress amplitude (log10) versus the number of cycles (log10) for heat-treated and untreated samples, respectively. Despite the inverse proportionality observed in both cases, the trends reveal key distinctions in the fatigue behavior of the samples under different treatment conditions. The coefficient of determination (R^2) for the fitted line plot of the untreated sample was higher than that of the heat-treated sample. This indicates that the data for the untreated sample exhibited a closer alignment with the fitted line, as depicted in Figure 8, than the heat-treated sample. Consequently, the software was able to generate a more accurate initial estimate for the *b* value of the untreated sample.

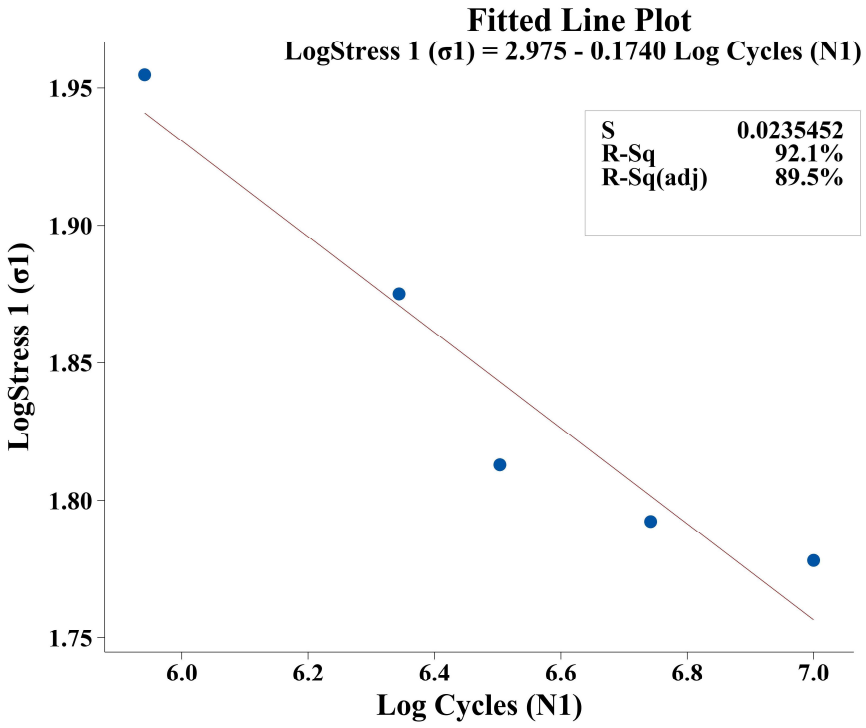

Figure 8. Fitted line plot of heat-treated samples.

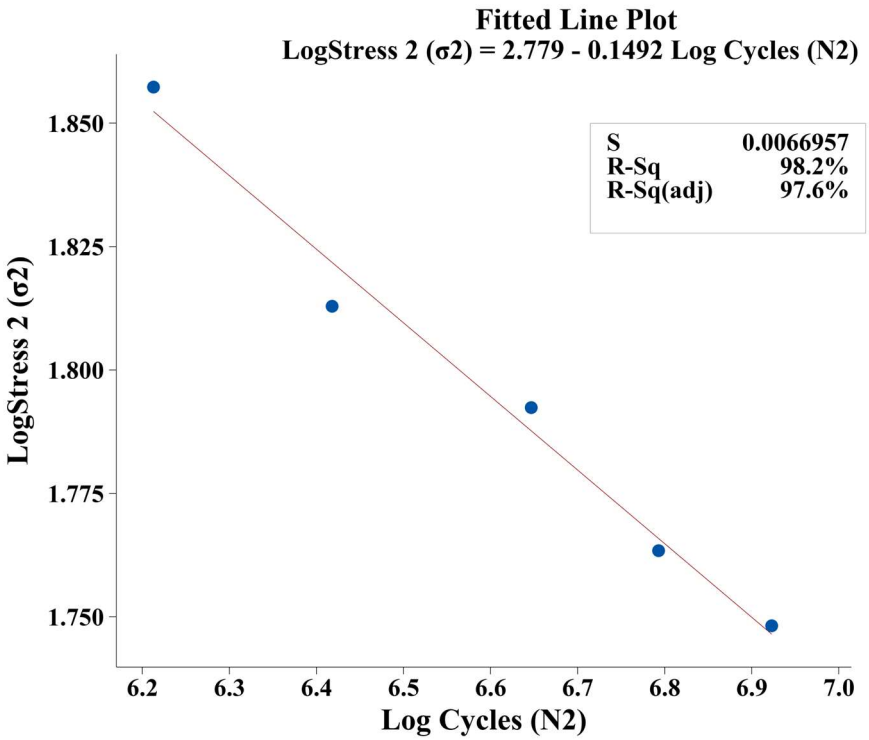

Figure 9. Fitted line plot of untreated samples.

The Gauss-Newton algorithm was used to fit a convex power equation like Basquin's. The algorithm was run for 200 maximum iterations with a tolerance setting of 0.00001, meaning that the algorithm would stop when the change in the parameters of the equation fell below 0.00001. The resulting equation was used to predict the composite's fatigue life under different stress conditions.

Minitab 21 software was used to plot the fatigue life results of heat-treated and untreated samples through a nonlinear regression fitted model, as shown in Figures 10 and 11. The convex power equation shows a correlation between stress amplitude and the number of cycles. Convex power in Eqs 6 and 7 represented the result of heat-treated and untreated samples. This equation can be expressed in the form of Basquin's equation, commonly used for fatigue life empirical modeling as follows. The coefficient of determination values for heat-treated and untreated fatigue life models are 99.68% and 99.84%, respectively. This indicates that a fatigue life prediction using the values of coefficient *A* and exponent *b* will result in an outstanding response.

$$\sigma r = 1107.27\ (N1)^{-0.184718} \tag{6}$$

$$\sigma r = 577.34\ (N2)^{-0.146349} \tag{7}$$

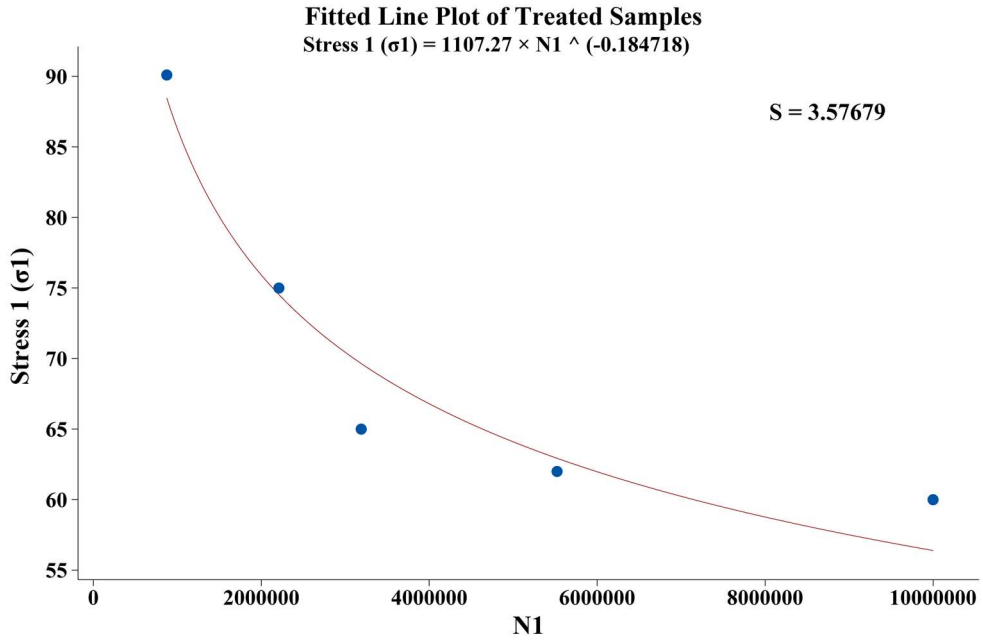

Figure 10. Fitted line plot of fatigue behavior of heat-treated samples.

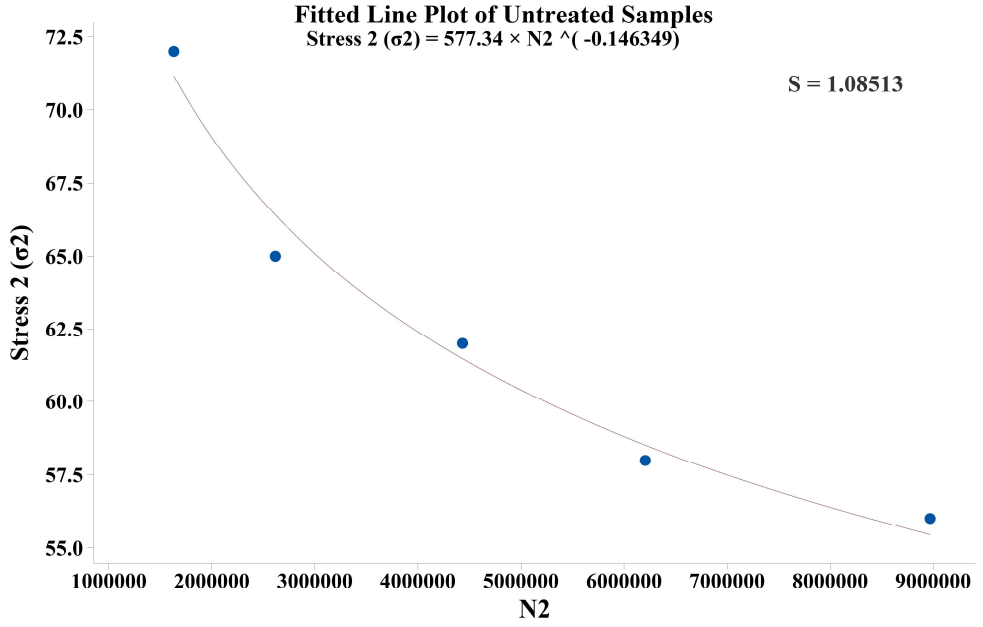

Figure 11. Fitted line plot of fatigue behavior of untreated samples.

3.6. Fracture surface examination

Fatigue-related fractography was studied to emphasize the relationship between the microstructure, crack initiation, and propagation behavior mechanisms. The fatigue fracture features were examined using a scanning electron microscope (SEM). SEM micrographs in Figure 12a reveal critical regions of fatigue crack initiation and the subsequent propagation direction. The crack propagation is characterized by the presence of fatigue striations, which indicate the cyclic loading nature of the material. The

development of cracks occurs through sub-structural and microstructural changes, ultimately leading to the coalescence of microcracks and the formation of dominant cracks. The arrows indicate the crack initiation zones and the direction of propagation. Additionally, sub-cracks within the primary region can be observed, reflecting the localized stress concentration responsible for crack initiation.

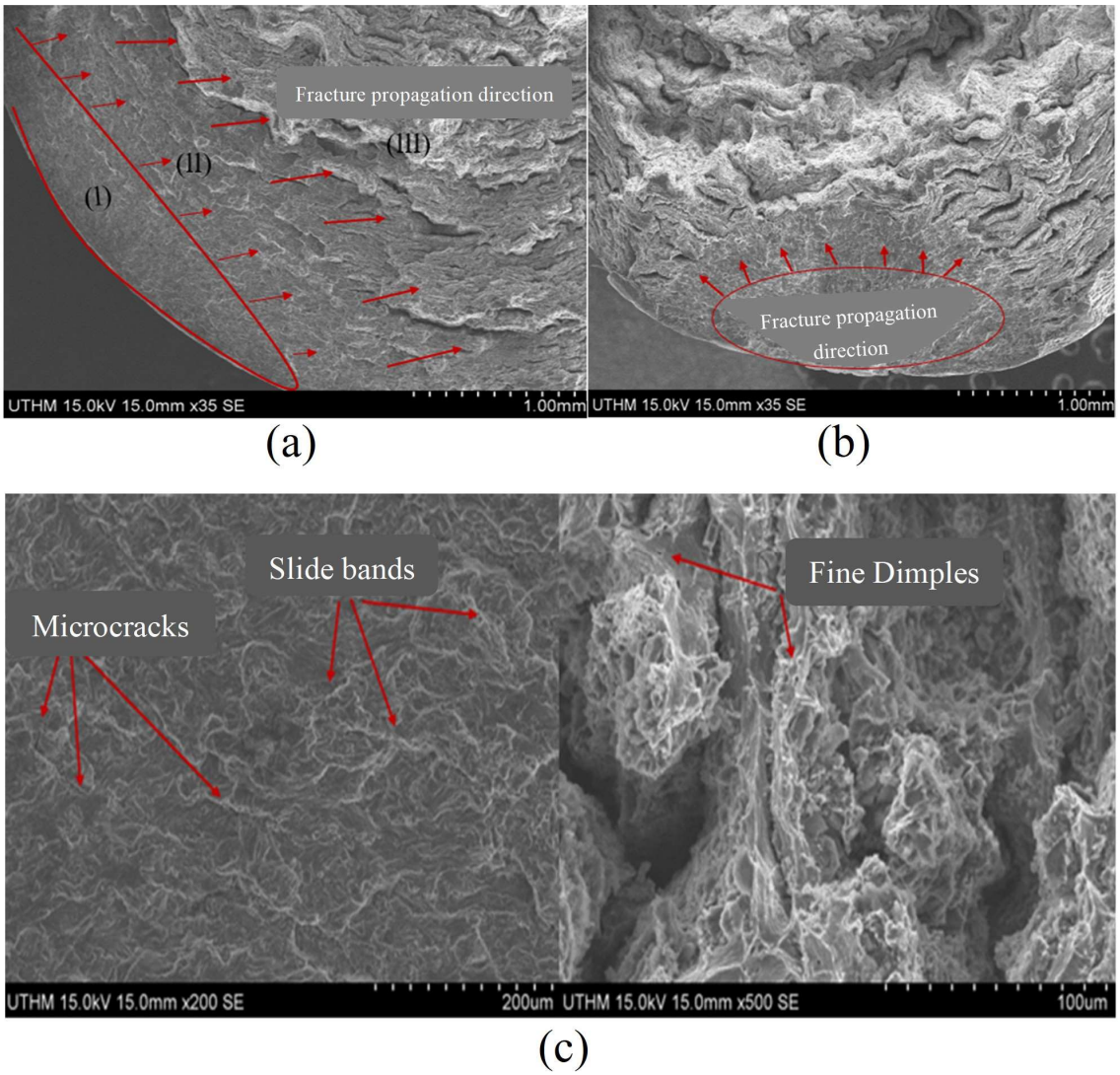

Figure 12. SEM micrographs of the HT fatigue fracture surface: (a) fatigue crack initiation, (b) the fracture propagation region, (c) fatigue fracture topology.

Figure 12b shows microstructural evolution contributing to crack growth, including reinforcement-derived particles originating from RHA and the aluminium matrix interface. These particles act as crack deflectors, redistributing stress and delaying crack propagation. Additionally, features such as crack branching and crack spacing are visible. This micrograph focuses on the fatigue fracture propagation. It highlights the gradual coalescence of microcracks, leading to larger dominant cracks. The arrows mark the fracture propagation direction, showing striations characteristic of fatigue crack growth. These features are consistent with plastic deformation mechanisms observed during fatigue testing.

At higher magnifications (e.g., Figure 12c), facet-like structures are observed at the fatigue crack initiation sites. These structures are inclined relative to the tensile axis and suggest localized plastic

deformation mechanisms at a magnification of ×500, such as necking and twinning. Fine dimples and microcracks further suggest ductile fracture behavior. Slide bands indicate strain localization under cyclic stress, whereas microcracks were developed before the final failure occurred.

The microstructural evidence demonstrates that in the HT samples, fatigue cracks initiate within the material's interior, irrespective of the reinforcement or heat treatment. However, the HT samples exhibit smaller crack initiation regions compared to the non-HT ones. The reduction in crack initiation zones suggests improved resistance to crack formation, attributed to the enhanced grain structure and precipitation strengthening achieved during heat treatment.

3.7. EDS analysis

EDS was used to identify and quantify elements in composite by analyzing the energy spectrum of X-rays emitted from the sample after exposure to a beam of electrons. Figure 13 presents the EDS analysis results of the Al6061 sample reinforced with 5% RHA. The analysis revealed that the sample comprises 86.02% Al, 9.65% Al_2O_3, 3.81% Si, and 0.91% Mg. The presence of Al_2O_3 is anticipated in aluminium alloys, as it naturally forms on the material's surface. The EDS results align with other samples extruded under similar conditions, suggesting minimal chemical composition variations due to the fixed extrusion temperature and RHA volume fraction. The presence of reinforcing phases revealed that silica-rich particles derived from RHA dispersed throughout the matrix. These particles hindered dislocation movement, thereby enhancing the material's resistance to crack propagation.

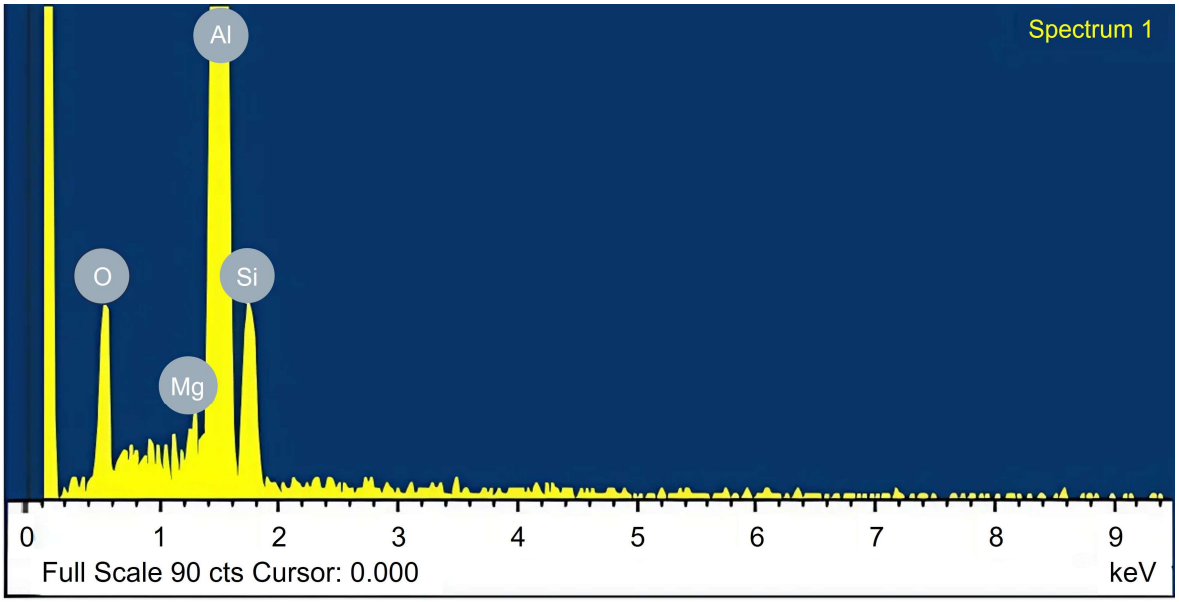

Figure 13. Diagram of EDS spectra with elemental analysis of the heat-treated sample.

3.8. Atomic force microscopy analysis

AFM is a widely used technique in materials characterization, providing high-resolution imaging and measurement of surface topography at micro- to nanoscale levels. AFM is utilized to study surface characteristics and grain structure in composite materials [31,32].

In this analysis, AFM was employed to examine the surface topography of heat-treated and untreated extruded samples. The mean grain area, defined as the projected surface area of the grain, ranged from 0.792 to 0.894 μm^2 for the heat-treated samples, while the mean grain area of the untreated samples ranged from 0.26 to 0.289 μm^2. The AFM analysis revealed that the heat-treated samples had a larger grain area than the untreated samples (Table 6). This increase in grain area is attributed to the grain growth phenomenon occurring when metal is heated, where grains can grow by absorbing atoms from neighboring grains, which may eventually disappear. The 3D images obtained from AFM listed in Tables 7 and 8 highlight the surface asperities of different topographical patterns, reflecting the effect of treatment conditions on surface topography. Differences in grain area and shape are visible, with treated samples exhibiting finer, closely packed grains (e.g., S1-HT), while NHT samples show larger, more separated grains (e.g., S8-NHT). The images illustrate a consistent trend of increasing grain area from untreated to treated samples, confirming the accuracy and repeatability of the AFM measurements.

The AFM analysis of Al/RHA composite samples highlights the significant impact of heat treatment on surface morphology and grain growth. Heat-treated samples exhibited reduced particle agglomeration and increased grain areas, as observed in the surface features, emphasizing the heat treatment's crucial role in refining the microstructure and improving the homogeneity of the composite material. This finding aligns with the expected microstructural changes during heat treatment, where grain coarsening occurs.

Table 6. AFM of mean grain size and surface roughness.

Sample No.	Mean grain area (μm^2)	Ra (nm)	Rq (nm)
SI-HT	0.855	7.654	6.089
S3-HT	0.792	9.451	7.498
S5-HT	0.894	8.635	6.825
S6-NHT	0.260	7.026	8.860
S8-NHT	0.289	6.533	5.252
S10-NHT	0.271	5.845	7.266

Table 7. AFM images of the heat-treated samples' topography.

Sample	AFM images of samples	Length histogram
S1-HT	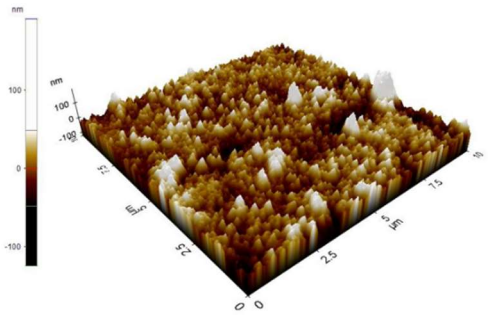	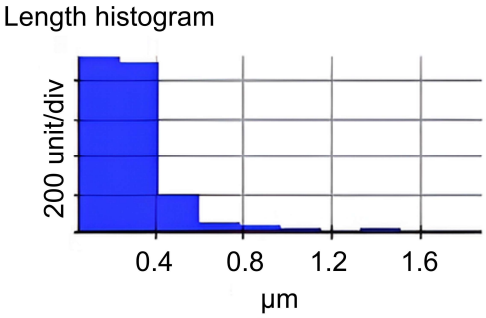
S3-HT	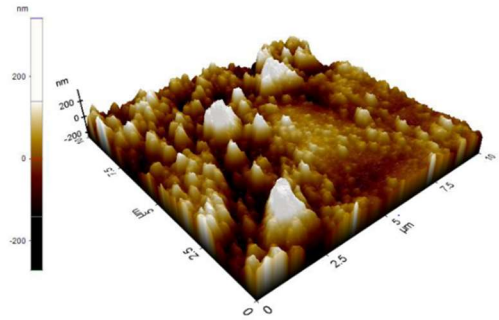	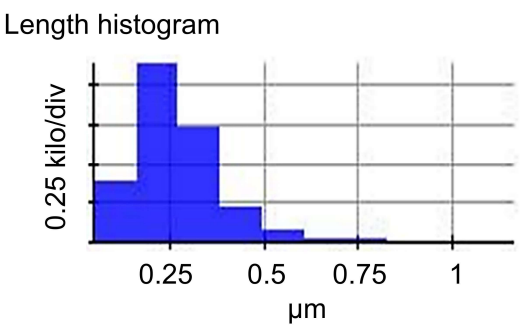
S5-HT	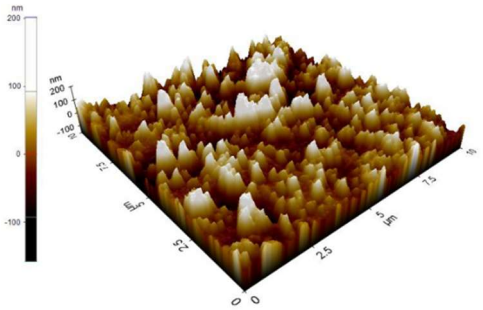	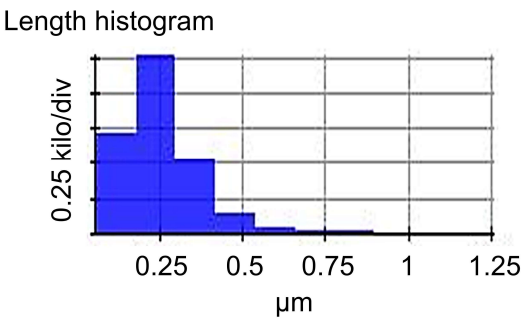

Table 8. AFM images of the untreated samples' topography.

Sample	AFM images of samples	Length histogram
S6-NHT	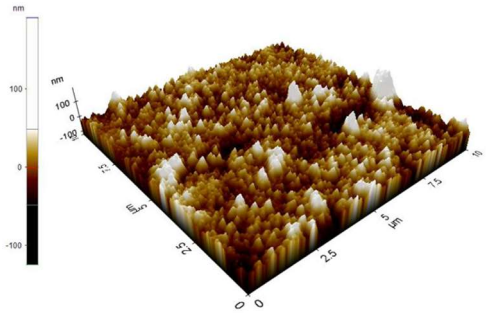	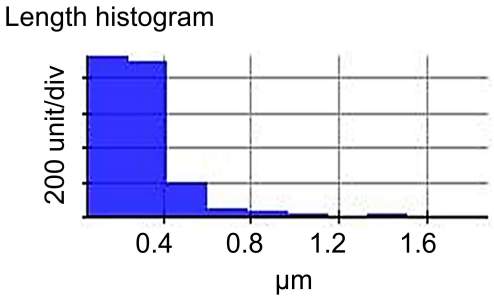
S8-NHT	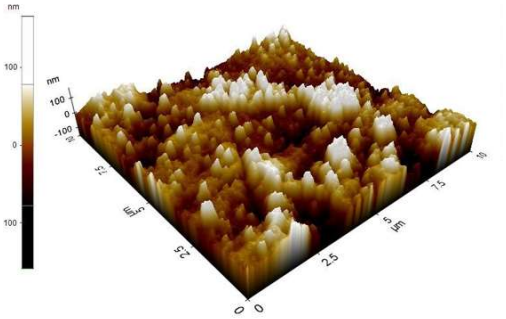	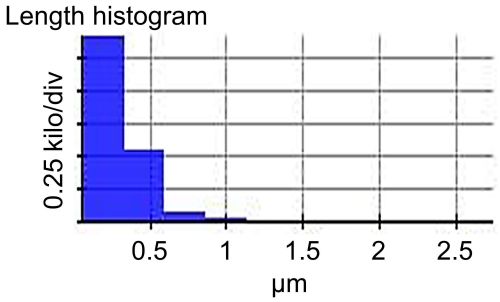
S10-NHT	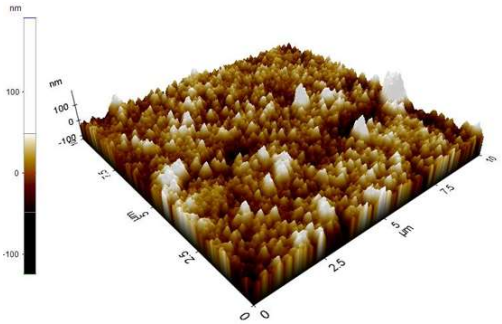	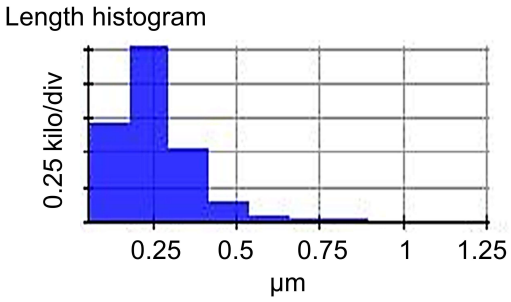

4. Conclusions

This study demonstrates that hot extrusion and heat treatment significantly improve the microstructure and mechanical properties of aluminium chip-based RHA-reinforced composites. The samples subjected to heat treatment exhibited enhanced tensile strength, hardness, and fatigue life relative to untreated samples. Adding RHA enhanced the mechanical properties of the samples. The reinforced, solution-treated, and aged samples exhibited higher strength and hardness than the unreinforced ones, attributed to the combined effects of fine grain refinement, improved particle-matrix bonding, and the precipitation of secondary phases during aging. The RHA particles enhance the composite's resistance to deformation and wear resistance owing to their inherent hardness and capability to obstruct dislocation movement. The solution treatment produced a more uniform microstructure characterized by fine-grain area, while the aging process promoted the precipitation of strengthening phases, resulting in enhanced strength and hardness. This study highlights the efficacy of direct recycling methods in waste reduction, cost savings, and environmental impact mitigation while simultaneously enhancing the quality of the final product. The findings can aid in developing more effective strategies

for recycling aluminium alloys and enhancing their properties through solid-state processing and heat treatment.

Use of AI tools declaration

The authors declare they have not used Artificial Intelligence (AI) tools in the creation of this article.

Acknowledgements

Communication of this research is made possible through monetary assistance by the Universiti Tun Hussein Onn Malaysia and the UTHM Publisher's Office via Publication Fund E15216. The authors express their profound appreciation for the supplementary provisions provided by the Sustainable Manufacturing and Recycling Technology, Advanced Manufacturing and Materials Center (SMART-AMMC), Universiti Tun Hussein Onn Malaysia.

Author contributions

Amin Shah Omar drafted the manuscript and conducted the experiments, including sample preparation and data collection. Shazarel Shamsudin conceptualized the research idea and oversaw data analysis and interpretation. Yahya M. Altharan contributed to the research methodology, critical review, and manuscript editing to enhance clarity and coherence. All authors read and approved the final manuscript.

Funding

This research was supported by the Universiti Tun Hussein Onn Malaysia (UTHM) through Tier 1 (Q390).

Conflict of interest

The authors declare no conflict of interest.

References

1. Mehtedi M El, Forcellese A, Mancia T, et al. (2019) A new sustainable direct solid state recycling of AA1090 aluminium alloy chips by means of friction stir back extrusion process. *Procedia CIRP* 79: 638–643. https://doi.org/10.1016/j.procir.2019.02.062
2. Raabe D, Ponge D, Uggowitzer PJ, et al. (2022) Making sustainable aluminium by recycling scrap: The science of "dirty" alloys. *Prog Mater Sci* 128: 100947. https://doi.org/10.1016/j.pmatsci.2022.100947
3. Canakci A, Varol T (2015) A novel method for the production of metal powders without conventional atomization process. *J Clean Prod* 99: 312–319. https://doi.org/10.1016/j.jclepro.2015.02.090

4. Altharan YM, Shamsudin S, Al-Alimi S, et al. (2024) A review on solid-state recycling of aluminium machining chips and their morphology effect on recycled part quality. *Heliyon* 10: e34433. https://doi.org/10.1016/j.heliyon.2024.e34433
5. Altharan YM, Shamsudin S, Lajis MA, et al. (2024) Optimizing strength of directly recycled aluminium chip-based parts through a hybrid RSM-GA-ANN approach in sustainable hot forging. *PLoS One* 19: e0300504. https://doi.org/10.1371/journal.pone.0300504
6. Zayed EM, Shazly M, El-Sabbagh A, et al. (2023) Deformation behavior and properties of severe plastic deformation techniques for bulk materials: A review. *Heliyon* 9: e16700. https://doi.org/10.1016/j.heliyon.2023.e16700
7. Mehtedi M El, Buonadonna P, Carta M, et al. (2023) Sustainability study of a new solid-state aluminium chips recycling process: A life cycle assessment approach. *Sustainability* 15: 11434. https://doi.org/10.3390/su151411434
8. Brough D, Jouhara H (2020) The aluminium industry: A review on state-of-the-art technologies, environmental impacts and possibilities for waste heat recovery. *Int J Thermofluids* 1–2: 100007. https://doi.org/10.1016/j.ijft.2020.100007
9. El-Garaihy WH, Alateyah AI, Shaban M, et al. (2023) A comparative study of a machine learning approach and response surface methodology for optimizing the HPT processing parameters of AA6061/SiCp composites. *J Manuf Mater Process* 7: 148. https://doi.org/10.3390/jmmp7040148
10. Anuar NFBW, Salleh MS, Omar MZ, et al. (2022) Mechanical properties and dry sliding wear behaviour of Al-Si-Mg alloy by equal channel angular pressing. *AIMS Mater Sci* 9: 733–749. https://doi.org/10.3934/matersci.2022045
11. Rymer LM, Winter L, Hockauf K, et al. (2021) Artificial aging time influencing the crack propagation behavior of the aluminium alloy 6060 processed by equal channel angular pressing. *Mater Sci Eng* A 811: 141039. https://doi.org/10.1016/j.msea.2021.141039
12. Tekkaya AE, Güley V, Haase M, et al. (2012) Hot extrusion of aluminium chips, In: Weiland H, Rollett AD, Cassada WA, *ICAA13 Pittsburgh*, Cham: Springer, 1559–1573. https://doi.org/10.1007/978-3-319-48761-8_235
13. Ab Rahim SN, Lajis MA, Ariffin S, et al. (2015) A review on recycling aluminium chips by hot extrusion process. *Procedia CIRP* 26: 761–766. https://doi.org/10.1016/j.procir.2015.01.013
14. Tekkaya AE, Schikorra M, Becker D, et al. (2009) Hot profile extrusion of AA-6060 aluminium chips. *J Mater Process Technol* 209: 3343–3350. https://doi.org/10.1016/j.jmatprotec.2008.07.046
15. Wagiman A, Mustapa MS, Asmawi R, et al. (2019) A review on direct hot extrusion technique in recycling of aluminium chips. *Int J Adv Manuf Technol* 106: 641–653. https://doi.org/10.1007/s00170-019-04629-7
16. Dhanesh S, Kumar KS, Fayiz NKM, et al. (2021) Recent developments in hybrid aluminium metal matrix composites: A review. *Mater Today Proc* 45: 1376–1381. https://doi.org/10.1016/j.matpr.2020.06.310
17. Seikh Z, Sekh M, Kunar S, et al. (2022) Rice husk ash reinforced aluminium metal matrix composites: A review. *Mater Sci Forum* 1074: 55–70. https://doi.org/10.4028/p-u8s016
18. Abolusoro OP, Khoathane MC, Washington W, et al. (2024) Mechanical and microstructural characteristics of recycled aluminium matrix reinforced with rice husk ash. *AIMS Mater Sci* 11: 918–934. https://doi.org/10.3934/matersci.2024044

19. Mohammed Usman A, Raji A, Waziri N, et al. (2014) Aluminium alloy-rice husk ash composites production and analysis. *LEJPT* 13: 84–98.
20. Yadav AK, Pandey KM, Dey A (2018) Aluminium metal matrix composite with rice husk as reinforcement: A review. *Mater Today Proc* 5: 1–7. https://doi.org/10.1016/j.matpr.2018.06.381
21. Seikh Z, Sekh M, Kibria G, et al. (2022) Density, hardness, and wear responses of rice husk ash reinforced aluminium composites. *Mater Sci Forum* 1074: 67–78. https://doi.org/10.1016/j.matpr.2021.04.318
22. Dixit P, Suhane A (2022) Aluminium metal matrix composites reinforced with rice husk ash: A review. *Mater Today Proc* 62: 4194–4201. https://doi.org/10.1016/j.matpr.2022.04.711
23. Joharudin NFM, Latif NA, Mustapa MS, et al. (2020) Physical properties and hardness of treated amorphous silica as reinforcement of AA7075 recycled aluminium chip. *IOP Conf Ser Mater Sci Eng* 864: 012015. https://doi.org/10.1088/1757-899X/824/1/012015
24. Olusesi OS, Udoye NE (2021) Development and characterization of AA6061 aluminium alloy/clay and rice husk ash composite. *Manuf Lett* 29: 34–41. https://doi.org/10.1016/j.mfglet.2021.02.005
25. Krolo J, Gudić S, Vrsalović L, et al. (2020) Fatigue and corrosion behavior of solid-state recycled aluminium alloy EN AW 6082. *J Mater Eng Perform* 29: 4310–4321. https://doi.org/10.1007/s11665-020-04975-8
26. Zupanič F, Klemenc J, Steinacher M, et al. (2023) Microstructure, mechanical properties and fatigue behaviour of a new high-strength aluminium alloy AA 6086. *J Alloys Compd* 941: 168976. https://doi.org/10.1016/j.jallcom.2023.168976
27. Hectors K, De Waele W (2021) Cumulative damage and life prediction models for high-cycle fatigue of metals: A review. *Metals* 11: 204. https://doi.org/10.3390/met11020204
28. Kwofie S (2001) An exponential stress function for predicting fatigue strength and life due to mean stresses. *Int J Fatigue* 23: 829–836. https://doi.org/10.1016/S0142-1123(01)00044-5
29. Kwofie S, Chandler HD (2007) Fatigue life prediction under conditions where cyclic creep–fatigue interaction occurs. *Int J Fatigue* 29: 2117–2124. https://doi.org/10.1016/j.ijfatigue.2007.01.022
30. Zhang Y, Zhang C, Sun K, et al. (2024) Test data evaluation of very high cycle fatigue based on maximum likelihood method. *J Phys Conf Ser* 2713: 012031. https://doi.org/10.1088/1742-6596/2694/1/012031
31. Al-Alimi S, Shamsudin S, Yusuf NK, et al. (2022) Recycling aluminium AA6061 chips with reinforced boron carbide (B_4C) and zirconia (ZrO_2) particles via hot extrusion. *Metals* 12: 1329. https://doi.org/10.3390/met12081329
32. Ruhaizat NE, Yusuf NK, Lajis MA, et al. (2022) Effect of direct recycling hot press forging parameters on mechanical properties and surface integrity of AA7075 aluminium alloys. *Metals* 12: 1633. https://doi.org/10.3390/met12101633